Vacuum 114 (2015) 142–149

Contents lists available at ScienceDirect

Vacuum

journal homepage: www.elsevier.com/locate/vacuum

Long-range structural correlations in amorphous ternary In-based oxides

Julia E. Medvedeva*, Rabi Khanal

Department of Physics, Missouri University of Science & Technology, Rolla, MO 65409, USA

ARTICLE INFO

Article history:
Received 11 September 2014
Received in revised form
14 October 2014
Accepted 5 November 2014
Available online 15 November 2014

Keywords:
Ab-initio molecular dynamics
Transparent amorphous oxides

ABSTRACT

Systematic investigations of ternary In-based amorphous oxides, In–X–O with X = Sn, Zn, Ga, Cd, Ge, Sc, Y, or La, are performed using ab-initio molecular-dynamics liquid-quench simulations. The results reveal that the local M–O structure remains nearly intact upon crystalline to amorphous transition and exhibit weak dependence on the composition. In marked contrast, the structural characteristics of the metal –metal shell, namely, the M–M distances and M–O–M angles that determine how MO polyhedra are connected into a network, are affected by the presence of X. Complex interplay between several factors such as the cation ionic size, metal–oxygen bond strength, as well as the natural preference for edge, corner, or face-sharing between the MO polyhedra, leads to a correlated behavior in the long-range structure. These findings highlight the mechanisms of the amorphous structure formation as well as the specifics of the carrier transport in these oxides.

1. Introduction

Although the unique properties of transparent amorphous oxide conducting and semiconducting materials were first demonstrated almost a decade ago [1,2], basic structural properties of these oxides – namely, the structural characteristics associated with the crystalline-to-amorphous transition – are far from understood. Most of the experimental characterization of the transparent amorphous oxides deal almost exclusively with the first shell, i.e., the coordination of oxygen atoms around metal cations [3–9]. Similarly, available theoretical models derived from molecular dynamics (MD) simulations of the amorphous oxides focus primarily on the Metal–Oxygen data with no or limited information on the Metal–Metal distances and coordination [10–18]. However, the first-shell remains nearly intact upon the crystalline-to-amorphous transition, owing to the strong oxygen electronegativity. Instead, integration of the Metal–Oxygen polyhedra into a continuous network – governed by the Metal–Metal distances, coordination, and oxygen sharing – plays a key role in the formation and properties of the amorphous oxides. Indeed, recent experimental and theoretical investigations of amorphous indium oxide [19] revealed that interconnectivity and spatial distribution of the InO polyhedra determines the electron transport limited by charge scattering: the observed peak in the electron mobility was found to correspond to the structure with long chains of InO_6 polyhedra connected primarily via corner sharing.

To gain a thorough systematic understanding of the role of composition in the structural properties of amorphous In-based oxides, eight ternary In–X–O structures with X = Sn, Zn, Ga, Cd, Ge, Sc, Y, or La, denoted below as a-IXO, were modeled using liquid-quench MD simulations. The choice for X cations in this study covers the typical compositional chemistry in both crystalline and amorphous transparent conducting and semiconducting oxides: all cations are pre- or post-transition metals with ns^0 electronic configuration. The structural characteristics of the first, second, and third shells as well as the connectivity between the MO polyhedra are compared for amorphous indium oxide (a-IO) and a-IXO. The results highlight the importance of the spatial distribution of the InO_6 and XO polyhedra from the point of view of amorphization and charge transport and facilitate the progress in fundamental understanding of amorphous oxides.

2. Computational method

The amorphous a-InO and a-InXO structures were generated using first-principles molecular dynamics as implemented in the Vienna Ab Initio Simulation package (VASP) [20–23]. The calculations are based on the density functional theory (DFT) [24,25] with

* Corresponding author.
E-mail address: juliaem@mst.edu (J.E. Medvedeva).

http://dx.doi.org/10.1016/j.vacuum.2014.11.006
0042-207X/

PBE functional based on the projector augmented-wave method [26–28]. For the initial structure, we used a cubic 130-atom cell of bixbyite In_2O_3 with density 7.12 gm/cm^3. To obtain ternary IXO structures, we randomly replaced 20% of the In atoms in the initial structure by respective metal X (Sn, Zn, Ga, Cd, Ge, Sc, Y or La) and adjusted (i) the number of oxygen atoms to maintain stoichiometry; and (ii) the cell volume to maintain the density in the In-based samples. The resulting lattice parameters that we have used in our studies are: 11.898 Å for InO; 12.11 Å for InSnO; 11.78 Å for InZnO; 11.80 Å for InGaO; 12.06 Å for InCdO; 11.86 Å for InGeO; 11.66 Å for InScO; 11.91 Å for InYO; and 12.17 Å for InLaO.

For each initial IO or IXO structure, we performed molecular dynamics simulations of liquid quench as follows. First, to remove any crystalline memory, each initial structure was melted at 3000 K for 6 ps. The melt was then cooled to 1700 K at the rate of 100 K/1.2 ps, and then rapidly quenched to 100 K at the rate of 200 K/1.2 ps. In order to make the calculations computationally efficient, we used low cut-off of 260 eV and restricted the *k*-point sampling to Γ point only during melting and quenching processes. Finally, each structure was equilibrated at 300 K for 6 ps with a cut-off energy of 400 eV. All simulations were carried out within NVT ensemble with Nose'-Hoover thermostat using integration time step of 2 fs.

3. Results and discussion

3.1. In–O and X–O distances in amorphous IO and IXO

To understand the role of composition in the structural properties of amorphous In-based oxides, first, the local structure of the InO_x polyhedra in a-IO and a-IXO with X = Sn, Zn, Ga, Cd, Ge, Sc, Y, or La, is analyzed. For this, the distribution of the In–O distances and the In coordination with oxygen atoms in a-IXO are compared to the corresponding In–O values in a-IO as well as those in crystalline In_2O_3. For an accurate comparison of the average In–O distances in a-IO and a-IXO, the average pair correlation function [29,30] was calculated according to:

$$l_{av} = \frac{\sum_i l_i \exp\left(1 - \left(\frac{l_i}{l_{\min}}\right)^6\right)}{\sum_i \exp\left(1 - \left(\frac{l_i}{l_{\min}}\right)^6\right)} \quad (1)$$

where the summation runs over all oxygen neighbors of a particular In atom and $l_{\min}$ is the smallest In–O distance in the *i*-th InO_x polyhedron. The results, shown in Fig. 1, reveal that the average pair correlation function increases for X = Sn, Zn, Ga, or Ge, and decreases for X = Cd, Sc, La, or Y, with respect to the In–O value in a-IO. The average In–O distance in all In-based oxides remains to be below the corresponding value in crystalline In_2O_3, namely, 2.18 Å. The shortest average In–O distance in case of a-IYO is in accord with the short In–O distance in crystalline hexagonal $YInO_3$, namely, 2.10 Å.

The above trends in the average In–O distance in a-IXO, Fig. 1, reveal no correlation with the ionic radii of the X cations. Indeed, the In–O distance cannot be affected directly by the presence of X cation since the In–O–M bond angle (M = In or X) is significantly less than 180° (on average, the In–O–M angles are equal to 98° and 116° for edge- and corner-shared In–M pairs, respectively.) For all X, the changes in the average In–O correlation function are insignificant, i.e., less than 1%. Moreover, the presence of X appears to have little effect on the radial In–O distance distribution: the calculated standard deviation, σ^2, shows only a small variation with composition, Fig. 1. The standard deviation increases for X = Ga or Ge which may be explained by their small ionic radii and the strength of the X–O bonds. A different mechanism should be sought for X = Sn in order to explain the increase of the average In–O distance and the distance distribution in a-ITO with respect to a-IO, c.f., Fig. 1. We believe that spatial distribution and connectivity of SnO_x and InO_6 polyhedra in a-ITO are important in determining the structural characteristics, as described below.

It is important to stress that local changes in the InO structure averaged out by the standard characterization procedures, Fig. 1, may be important from the crystallization and charge transport points of view. In particular, the strength of the X–O bonds with respect to that of the In–O bond (the so-called "oxygen-getter" behavior of X cation [31]) may affect the local In–O structure: (i) by introducing a "ripple" effect when the In–O bond distance fluctuates with the number of X neighbors [32]; and (ii) by changing the relative contributions from the differently coordinated In atoms (discussed below). Clearly, the spatial distribution of XO polyhedra within the InO framework (e.g., clustering *vs* uniform distribution of XO) becomes critical in determining the crystalline to amorphous transition as well as the transport properties (conductivity paths and scattering) in multicomponent oxides and will be addressed below.

The calculated average pair correlation function l_{av}(X–O), Eq. (1), for each a-IXO structure is given in Fig. 2. The results reveal that for X = Sn, Cd, Ge, Sc, or Y (for X = Zn, Ga, or La), the average X–O distance is shorter (longer) than the natural X–O distance, i.e., the distance in the corresponding crystalline binary oxides. Interestingly, the X–O distances in the available crystalline ternary In-containing oxides (we considered $In_4Sn_3O_{12}$, In_2ZnO_4, $GaInO_3$,

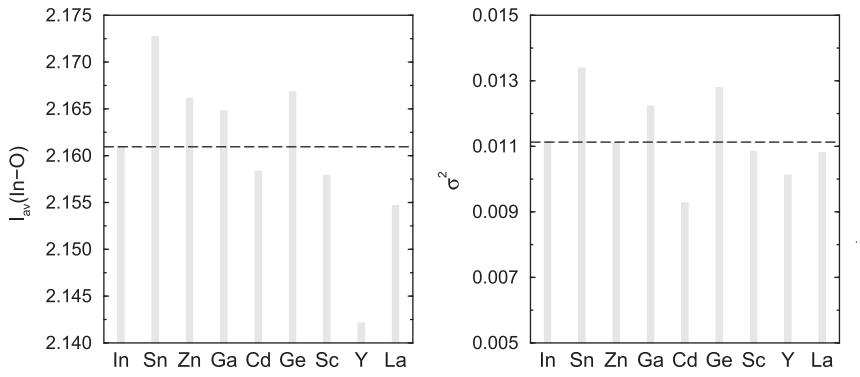

Fig. 1. (Left) Calculated average In–O pair correlation function, l_{av}, in Å, for amorphous IO and IXO. (Right) Calculated standard deviation of the radial In–O distance distribution, σ^2, in Å^2, for amorphous IO and IXO. The horizontal dash lines represent the corresponding values in amorphous IO.

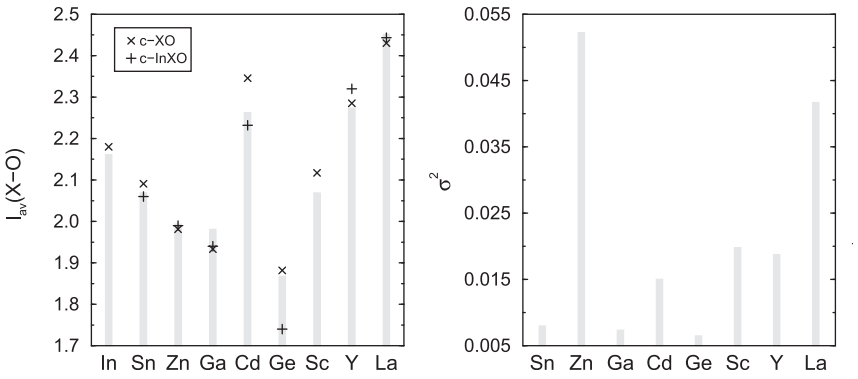

Fig. 2. (Left) Average X–O correlation function, l_{av}, in Å, in amorphous IXO. Also, the X–O distance in the corresponding crystalline binary (cross) and In-containing ternary (plus) oxides are given for comparison. (Right) Calculated standard deviation of the radial X–O distance distribution, σ^2, in Å^2, for amorphous IXO.

$CdIn_2O_4$, $In_2Ge_2O_7$, $YInO_3$, and $LaInO_3$; all structural properties found in the Inorganic Crystal Structure Database), in general, predict the average X–O distances in a-IXO rather well (e.g., for X = Sn, Zn, Cd, or La). However, the preference of the X cation to have a particular oxygen coordination should be taken into consideration. For example, about a half of Ge atoms are found to be six-coordinated in a-IGeO (similar to rutile GeO_2) whereas Ge is four-coordinated with oxygen atoms in $In_2Ge_2O_7$; hence, the Ge–O distance in a-IGeO deviates significantly from that in $In_2Ge_2O_7$, Fig. 2.

In marked contrast to the small variation in the standard deviation for the In–O distances in a-IXO, Fig. 1, the X–O distance distribution is narrow only for X = Sn, Ga, and Ge, Fig. 2. (Note that the the standard deviation for the In–O distances is large for these three cases, Fig. 1). The calculated standard deviation, σ^2, is above 0.015 Å^2 for X = Cd, Sc, and Y, that is notably larger than the corresponding In–O value in a-IXO (c.f., Fig. 1). Most significantly, the standard deviation is above 0.04 Å^2 and 0.05 Å^2 for X = La and Zn, respectively. The corresponding radial X–O distributions are asymmetric towards longer distances, i.e., there is an appreciable amount of long-distance Zn–O and La–O bonds. This finding may be explained by the Zn and La tendency to be over-coordinated: many Zn and La atoms acquire higher than natural coordination in a-IXO (see below). This is in accord with crystalline oxides: La has 8 oxygen neighbors in $InLaO_3$ and Zn is 5-coordinated in crystalline multicomponent oxides [33,34]. The presence of the long-distance X–O bonds may favor connectivity between the XO polyhedra via corner-sharing – as opposed to isolated short-bonded polyhedra or clusters of edge-shared polyhedra.

3.2. In–O and X–O coordination in amorphous IO and IXO

Based on the obtained pair correlation function (Eq. (1)), the effective coordination number (ECN) can be calculated as follows:

$$\mathrm{ECN} = \sum_i \exp\left(1 - \left(\frac{l_i}{l_{av}}\right)^6\right). \qquad (2)$$

The average effective coordination numbers calculated for a-IXO, Fig. 3, reveal that indium is under-coordinated with oxygen atoms in all In-based amorphous oxides – as compared to the crystalline In_2O_3 with 6-coordinated In atoms. Moreover, at 20% substitution, all X additions considered in this work have little effect on the average In–O coordination changing it only slightly as compared to <ECN>=5.0 in a-IO: Sn, Zn, Ga, and Y result in <ECN> ~ 5.1, whereas Ge and Sc increase it to <ECN> ~ 5.3. La has the smallest effect on the average In coordination whereas Cd decreases it to 4.98.

Although the average In–O coordination remains nearly unchanged in a-IXO, the statistical distribution of the In coordination, i.e., the relative number of differently coordinated In atoms, reveals a strong dependence on the composition. Within a radial distance of 2.36 Å from a central In atom (to be compared to the longest In–O distance in the first shell in crystalline In_2O_3, 2.25 Å), there are 3, 4, 5, and 6-coordinated In atoms, denoted below as InO_x, Fig. 4. In

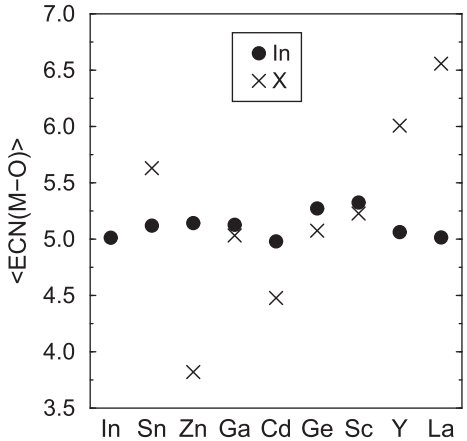

Fig. 3. Average effective coordination number of In and X with oxygen atoms in amorphous IO and IXO.

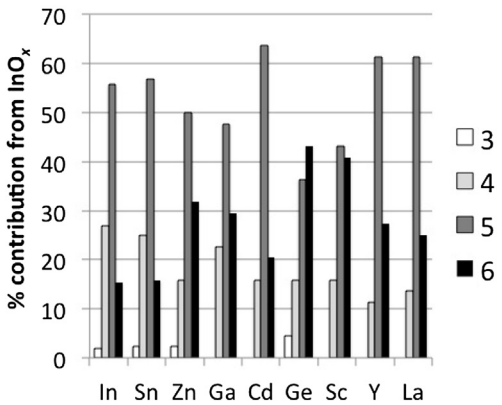

Fig. 4. Relative number of differently coordinated indium atoms in amorphous IO and IXO calculated within 2.36 Å around a central In atom.

a-IO and all a-IXO except for IGeO and IScO, most of the In atoms (around 50% or above) are 5-coordinated. The number of 6-coordinated In atoms in a-IXO suggests a particular grouping of the addition elements. Specifically, Sn stands apart from the other X additions since it has the least effect on the In coordination statistics. X = Cd, Y, and La result in an increase of both the 5- and 6-coordinated In atoms. In contrast, for X = Zn, Ga, Ge, and Sc, only the number of 6-coordinated In increases – up to 30% for Zn or Ga and up to 40% for Ge and Sc. Hence, addition of Ge or Sc leads to the most pronounced tendency to fulfill the natural In coordination. As discussed below, spatial distribution and connectivity of the InO_6 plays the key role during amorphization of In-based oxides and may also govern the charge transport.

In contrast to under-coordinated In, the average coordination of all the addition elements except for Cd and Sc is close to their natural coordination, i.e., the coordination in the corresponding crystalline binary oxides. In a-IXO, Ga and Ge are, on average, 5-coordinated (both can be found 4 and 6-coordinated in binary oxides); Y and La reach or exceed their natural coordination of 6; Sn and Zn are close to being 6- or 4-coordinated, respectively, in accord with their coordination in binary oxides. Only Sc and especially Cd are notably under-coordinated; both have the natural coordination of 6 in the corresponding binary oxides. We note that the low coordination of Cd in amorphous ICdO (4.5) is in accord with crystalline ternary oxide In_2CdO_4 where Cd is four-coordinated. This may be explained by weaker Cd–O bonds as compared to the In–O bonds.

3.3. In–M coordination and distances

Amorphous oxide structure can be considered as a network of distorted MO polyhedra. A thorough understanding of the In–M shell structure, i.e., the average In–M distances and In–O–M angles, provides valuable information about interconnectivity between the MO polyhedra. However, characterization of the In–M shell is challenging. The proximity of the second and third shells in the crystalline In_2O_3 associated with six edge-shared In–In bonds at ~3.35 Å and six corner-shared In–In bonds at ~3.83 Å, respectively, leads to significant overlap of the corresponding distribution functions in amorphous indium oxide [19]. Hence, it is hard to distinguish between the second and third shells from a measured general pair distribution function. Moreover, the total In–M distance distribution becomes over 1 Å wide, making the exponential fit in the l_{av} and ECN calculations, Eqs. (1) and (2), inapplicable in this case.

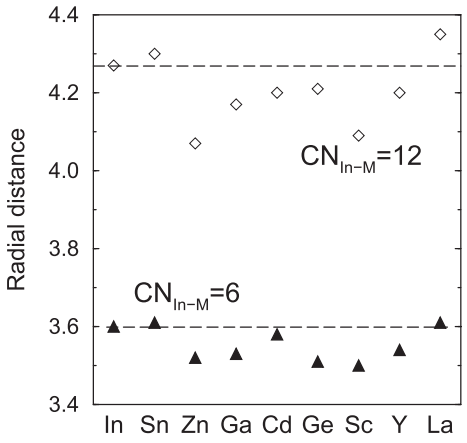

Fig. 5. Radial distance, in Å, from a central In atom at which the average In–M coordination number becomes 6.0 (triangles) and 12.0 (diamonds) in a-IO and a-IXO. The horizontal dash line corresponds to the values for a-IO and is given to guide the eye.

Independent of the type of sharing (edge vs corner), the total In–M coordination (or running coordination) can be calculated as a function of the distance from a central In atom. In amorphous IO, it reaches the expected 6.0 (12.0) at ~3.6 Å (4.3 Å), i.e., above the crystalline In_2O_3 value of 3.4 Å (3.8 Å). Addition of Ga, Zn, Ge, Sc, Y or Cd increases the total In–M coordination as compared to that in a-IO, whereas Sn or La slightly reduces it, Fig. 5. These results do not correlate with the ionic size of the X cation: the ionic radius of La (1.17 Å) is the largest among all X cations considered, while the ionic radius of Sn (0.83 Å) is smaller than that of In (0.94 Å) as well as of Sc (0.89 Å), Y (1.04 Å), or Cd (1.09 Å). The Sn- or La-induced decrease of the total In–M coordination is in accord with the longest average In–O distance in a-ITO, Fig. 1, and the strong tendency of La toward over-coordination in a-ILaO, Fig. 3.

To distinguish between the edge- and corner-shared In–M pairs, we determine the number of metal neighbors (In or X) that share one, two, or three oxygen atoms with a central M atom. The resulting In–M coordination numbers represent the number of corner, edge, or face-shared metal atoms, respectively, for every M atom. In this analysis, one should choose a maximum metal–O distance to be considered as M–O bond in the metal–metal sharing – this cut-off value should ensure that the first shell M–O distances in the corresponding pair distribution function (i.e., those that belong to the first In–O or X–O peak) are included into consideration. In our analysis, we set the cut-off values to 2.36 Å for In–O bond and Sn–O bond; 2.20 Å for Zn–O bond and Ga–O bond; 2.10 Å for Ge–O bond; 2.27 Å for Sc–O bond; 2.44 Å for Y–O bond; 2.55 Å for Cd–O bond; and 2.75 Å for La–O bond. As a result, average M–M distance and M–O–M angle for edge-, corner-, and face-shared M–M pairs are derived for each oxide.

First of all, we find that addition of X = Sn or Cd does not change the relative number of the edge-*vs* corner-shared In–In pairs which is 15% *vs* 85%, respectively, of the total shared In–In pairs in a-IO as well as in a-ITO and a-ICdO. The number of edge-shared In–In pairs increases to 19–21% for all other X cations. The low number of edge-shared In–In pairs in In-based oxides (about a half of the edge-shared pairs become corner-shared upon amorphization) does not translate into a low mobility in amorphous oxides. Indeed, the observed mobility peak in a-IO was found to correspond to the structure with the *smallest* edge-shared In–In coordination number [19]. This counter-intuitive result was explained by the abundance of long-distance corner-shared In–In pairs that enables formation of long chains of connected InO_6 polyhedra [19]. The extended InO_6 chains (as opposed to InO_6 clusters of edge-shared polyhedra) are believed to be responsible for lower scattering and, hence, an improved mobility.

The average In–In distance and In–O–In angle for both edge- and corner-shared In–In pairs in a-IO and a-IXO are given in Fig. 6. There is a correlation between the average In–In distance for edge-shared and corner-shared In–In pairs: a shorter edge-shared distance generally correspond to a longer corner-shared distance, and vice versa. Accordingly, the average In–O–In angles for the edge-shared and corner-shared In–In pairs show a clear correlation, Fig. 6(b). However, the effect of X is more complex: only X = Sn, Sc, or Y reduce the average edge-shared In–In distance, whereas all X additions increase the average corner-shared In–In distance as compared to those in a-IO. The longest corner-shared In–In distance in a-ITO and a-ILaO is in accord with the increased total In–M coordination which may be explained by the Sn and La tendency toward overcoordination and clustering. Therefore, owing to the higher degree of freedom, the corner-shared In–In pairs serve to compensate changes in the edge-shared shell (if any) as well as to adjust to the presence and spatial distribution of XO polyhedra.

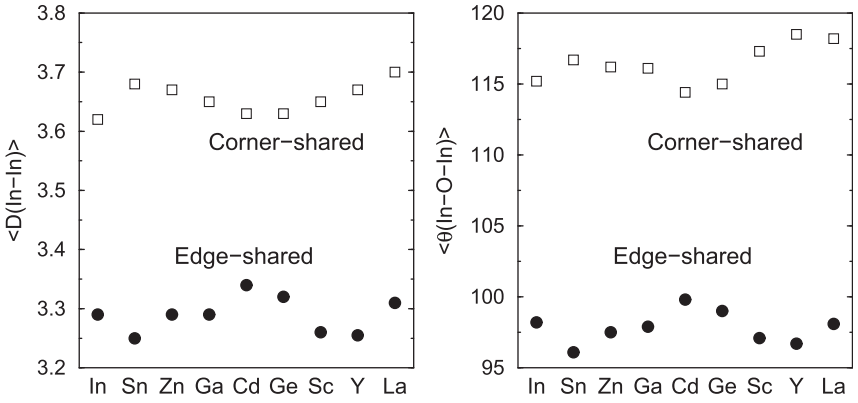

Fig. 6. Average In–In distance, in Å (left) and average In–O–In angle, in degrees, (right) for edge-shared (circle) and corner-shared (square) In–In pairs in amorphous IO and IXO. For comparison, the crystalline In_2O_3 edge-shared and corner-shared In–In distances are 3.4 Å and 3.8 Å, respectively, and average In–O–In angles are 99–101° and 126°, respectively.

3.4. InO_6 connectivity and spatial distribution

The reduced number of edge-shared In–In pairs in the amorphous In-based oxides signifies changes in the connectivity between InO polyhedra upon crystalline-to-amorphous transition. For amorphous InO, it has been shown that the size and distribution of nanocrystalline In_2O_3 inclusions which are present in the amorphous oxide samples even below the transition to the so-called "X-ray amorphous" state, limit the transport properties via scattering [19]. Nucleation of such nanocrystallites was found in amorphous InO structures obtained via MD simulations at slow cooling rates (5 K/ps), and it was shown that the spatial distribution of the InO_6, i.e., homogeneous distribution of separate-standing (i.e., not connected) InO_6 polyhedra vs chains vs clusters, depends strongly on the deposition temperature in PLD-grown samples or quench rates in MD simulated structures and ultimately determines the properties of amorphous indium oxide [19]. In this work, the MD quench rates employed for a-IO and a-IXO (170 K/ps) are expected to be fast enough to prevent InO_6 clustering and, hence, to avoid nucleation of In_2O_3 nanocrystallites. Indeed, in a-IO obtained at this cooling rate, only 13% of In atoms are 6-coordinated, and these InO_6 are distributed uniformly throughout the cell volume: the number of connected InO_6 (via edge or corner-sharing) is small, Fig. 7, and the average distance between shared InO_6 polyhedra is 3.68 Å which is greater than the average shared In–In distance in crystalline In_2O_3, 3.6 Å. The latter is primarily due to the presence of long-distance corner-shared InO_6–InO_6 pairs that result in the average corner-shared In_6–O–In_6 angle of 138° (to compare, the average corner-shared In–O–In angle in crystalline In_2O_3 is 126°).

Significantly, all X cations considered in this work except for Sn increase the number of 6-coordinated In atoms, Fig. 4. The number of connected InO_6 polyhedra increases accordingly, Fig. 7, but composition also affects the way the InO_6 polyhedra connect with each other, i.e., the relative number of edge-vs corner-shared In_6–In_6 pairs is different in a-IXO, Fig. 7. In particular, although Sn has little effect on the fractional number of 6-coordinated In atoms, Fig. 4, it affects the spatial distribution of the In_6 atoms by suppressing the number of edge-shared InO_6 polyhedra, Fig. 7. At the same time, Sn leads to the formation of short-distant edge-shared In_6 pairs (~3.1 Å) that results in the smallest average distance between connected In_6–In_6, Fig. 7. The effect of composition is manifested clearly when the InO_6 features are compared for a-IZO and a-IGO. In these oxides, the relative number of 6-coordinated In atoms is nearly the same (and doubled as compared to a-IO and a-ITO, Fig. 4); however, Zn promotes edge-sharing between the InO_6 polyhedra whereas Ga favors their corner-sharing, Fig. 7. Such differences in the InO_6 connectivity are likely to reflect different charge transport in a-IZO and a-IGO.

The average In_6–In_6 distance for the connected InO_6 polyhedra in a-IXO varies with composition: it increases for X = Ga or La; decreases for X = Sn, Zn, or Sc; and remains similar to that in a-IO

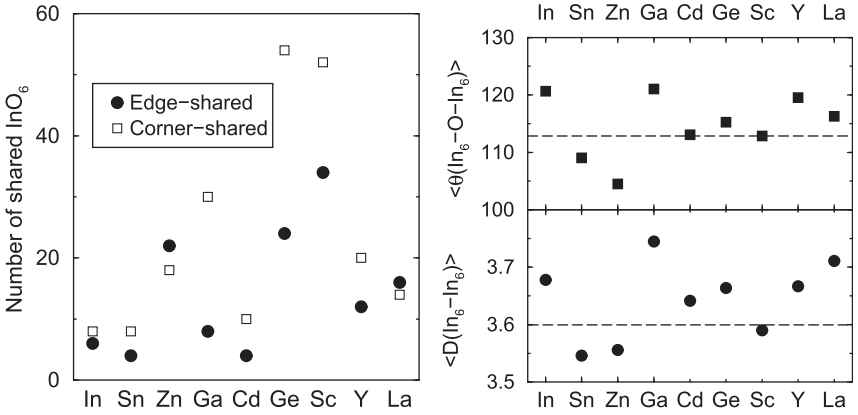

Fig. 7. (Left) Number of edge-shared and corner-shared In_6–In_6 pairs in amorphous IO and IXO. (Right) Average In_6–In_6 distance, in Å, and average In_6–O–In_6 angle, in degrees, for the InO_6 polyhedra connected via edge- and corner-sharing in amorphous IO and IXO. The horizontal dash line represents the corresponding values averaged for the second and third shells in crystalline In_2O_3.

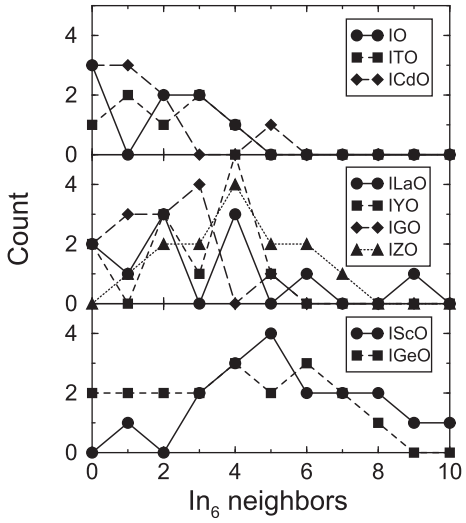

Fig. 8. The probability of the number of In_6 neighbors calculated within a radial cut-off distance of 3.8 Å from a central In_6 in a-IO and a-IXO. The oxides are grouped according to the fractional number of the 6-coordinated In atoms, c.f., Fig. 4, that is ~20% for a-IO, a-ITO, and a-ICdO; ~30% for a-ILaO, a-IYO, a-IGO, and a-IZO; ~40% for a-IScO, and a-IGeO.

for X = Ge, Y, or Cd, Fig. 7. The variation does not follow the trend in the fractional number of In_6 (c.f., Fig. 4) and does not correlate with the ionic size of X. This finding highlights that different composition-dependent mechanisms are responsible for the formation of the amorphous oxide structure, and also may signify a tendency toward InO_6 clustering in some a-IXO. To verify this assumption, the number of In_6 neighbors was calculated within a radial cut-off distance of 3.8 Å from a central In_6. (Note that oxygen sharing, i.e., connectivity between the InO_6 polyhedra, was not taken into account in these calculations, and the distance of 3.8 Å is simply to include the In–In distance of the second and third shells in crystalline In_2O_3). The results are grouped according to the fractional number of 6-coordinated In atoms (c.f., Fig. 4) for comparison. One can see, Fig. 8, that addition of Cd increases the probability of finding 5 In_6 neighbors as compared to a-IO. For X = Y, La, Ga, and Zn, the fractional number of In_6 increases to about 30%, yet the spacial distribution of the InO_6 polyhedra is different: in a-IGO and a-IYO, the number of In_6 neighbors does not exceed 5, whereas in a-ILaO there is a cluster of as many as 9 In_6 neighbors. Amorphous IZO has a bell-shape distribution of In_6 neighbors, Fig. 8, with 4 In_6 neighbors to be the most likely arrangement. Finally, the spatial distribution of InO_6 polyhedra in a-IGeO appears to be more uniform than that in a-IScO: the probability to find a In_6 cluster of any size (no or 1 to 8 neighbors) is nearly the same in a-IGeO, whereas presence of Sc results in the largest InO_6 cluster of 10 neighbors, Fig. 8. We must stress here that the role of oxygen-non-stoichiometry and deposition temperatures (or cooling rates) on the structural properties of a-IXO was not taken into account in this work. Such investigations are ongoing and are expected to elaborate the effect of X addition.

3.5. XO connectivity and spatial distribution

At 20% fraction of X, the spatial distribution and connectivity of XO polyhedra are expected to play a more important role in charge scattering than the distribution of InO_6 polyhedra discussed above. In Fig. 2, a tendency toward the X–O natural distances (i.e., those found in the crystalline binary counterparts) has been demonstrated. Here, the second and third shells, i.e., X–X distances and X–O–X angles, as well as the type of sharing between the connected XO polyhedra are analyzed. First, we find that the number of shared XO polyhedra correlates with the X ionic radius: for X = Zn, Ga, Ge, or Sc with a small ionic radius, there are 12–14 connections per cell, whereas for X = Sn, Cd, Y, or La with a large ionic radius, the total number of connections increases to 20–24, Fig. 9. Furthermore, the average X–X distances and average X–O–X angles for the connected XO polyhedra in a-IXO, Fig. 9, resemble those found in the corresponding crystalline counterparts.

In addition to the expected cation size effect on the connectivity between XO polyhedra, we find that some X cations have a strong preference for either corner or edge sharing of the XO polyhedra. Specifically, no edge-shared Zn–Zn or Ge–Ge pairs are found in a-IZO and a-IGeO, in excellent agreement with crystalline binary (wurtzite ZnO and cristobalite GeO_2) as well as ternary (In_2ZnO_4 and $In_2Ge_2O_7$) oxides. On the other hand, Ga and La favor edge sharing so that the fractional number of the edge-shared Ga–Ga or La–La is significantly larger than that of corner-shared, Fig. 9. In a-ILaO, La also promotes face-sharing between LaO polyhedra (four La–La pairs were found to share three oxygen atoms) that is likely to be associated with La strong tendency toward over-coordination. In a-IGO, the strong preference for edge-sharing leads to the formation of GaO clusters, Fig. 10 – in marked contrast to a homogeneous distribution of ZnO and GeO polyhedra with a similar number of connected XO polyhedra in amorphous IZO, IGO and IGeO, Fig. 9. Similarly, a larger number of edge-shared Sn–Sn connections as compared to X = Cd, Fig. 9, signifies SnO polyhedra

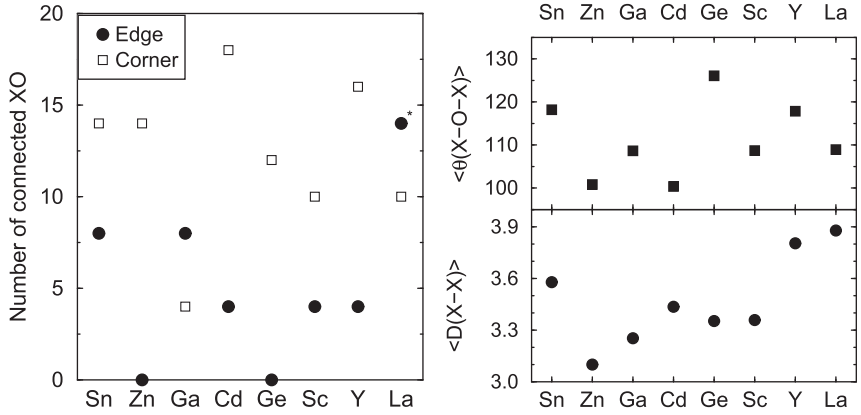

Fig. 9. (Left) Number of edge-shared and corner-shared X–X pairs in amorphous IXO. (Right) Average X–X distance, in Å, and average X–O–X angle, in degrees, for the XO polyhedra connected via edge- and corner-sharing in IXO.

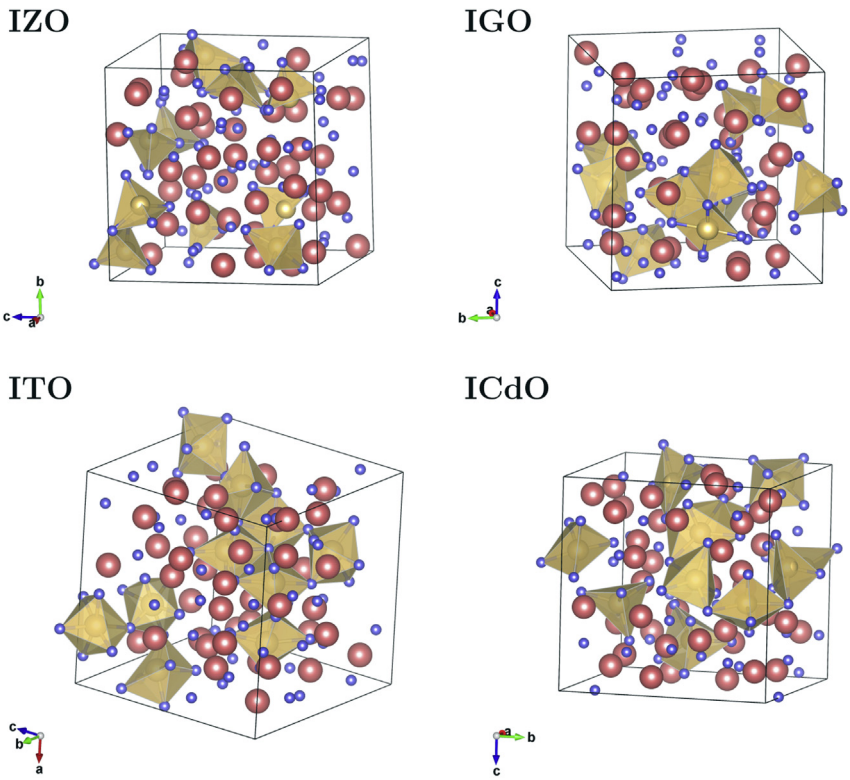

Fig. 10. Atomic structures of a-IXO, X = Zn, Ga, Sn, or Cd, highlighting the X–O bonds and XO polyhedra only. Small spheres represent oxygen atoms, and large spheres that are not connected with oxygen atoms represent In atoms.

clustering: indeed, five SnO_6 polyhedra connected via edge-sharing with the rest of the SnO_6 polyhedra attached via corner-sharing are found in a-ITO, Fig. 10. This finding may be explained by the Sn strong ability to attain full coordination with oxygen atoms as compared to In atoms that are more adaptable to distortions (this is opposite to Cd atoms that accept very low coordination with oxygen atoms, Fig. 3). Indeed, in the crystalline $In_4Sn_3O_{12}$, a fraction of Sn atoms form regular SnO_6 polyhedra, whereas all In atoms have a low symmetry coordination with the In–O distances ranging from 2.07 Å to 2.31 Å. Therefore, Sn addition may help to attain amorphous In-based oxide structure by distorting the InO polyhedra and, hence, preventing InO_6 clustering and the subsequent formation of In_2O_3 nanocrystallites. On the other hand, Sn has a strong tendency to cluster itself which ultimately limits the electron mobility as the fraction of Sn increases. Further investigations of the role of oxygen-non-stoichiometry and cooling rates on the spatial X distribution in amorphous In-based oxides are expected to shed additional light on the tunable properties of oxides and are in progress.

4. Conclusions

The results of ab-initio molecular-dynamics liquid-quench simulations for eight ternary In-based amorphous oxides, a-IXO with X = Sn, Zn, Ga, Cd, Ge, Sc, Y, or La, reveal that several factors, ranging from local (ionic size and metal–oxygen bond strength) to long-range (natural preference for connectivity between MO polyhedra), play an important role in the structural properties of a-IXO and result in a complex composition-dependent behavior.

The local structure of the MO polyhedra remains, on average, nearly unchanged upon the transition from crystalline to amorphous state. Moreover, the average In–O coordination is 5.0–5.2 in a-IO and all a-IXO considered in this work. Such a weak dependence of the In coordination on composition may signify that In atoms remain to serve as a main source of oxygen defects upon fractional substitution with X. However, charge transport in a-IXO is likely to be affected strongly by the composition-dependent distribution of the InO_6 and XO polyhedra. Presence of X may result in a random distribution of the MO polyhedra or facilitate the formation of corner-shared chains or edge-shared clusters of the InO_6 and XO polyhedra that, in turn, will affect (i) the degree of amorphization of the In-based framework, and (ii) the carrier mobility controlled by scattering on large XO clusters or nanocrystalline inclusions. Preferred long-range distribution of MO polyhedra may also affect the mechanical properties of amorphous oxides.

Further investigations of the role of oxygen non-stoichiometry and deposition temperatures (or cooling rates) on the structural properties of a-IXO are expected to elaborate the effect of X addition on the carrier concentration and carrier transport.

Acknowledgments

The work was performed under the collaborative MRSEC program at Northwestern University and supported by the National Science Foundation (NSF) grant DMR-1121262. Computational resources were provided by the NSF-supported XSEDE program, grant TG-DMR080007.

References

[1] Bellingham J, Phillips W, Adkins C. Electrical and optical properties of amorphous indium oxide. J Phys Condens Matter Sci Lett 1990;2:6207–21.
[2] Nomura K, Ohta H, Takagi A, Kamiya T, Hirano M, Hosono H. Room temperature fabrication of transparent flexible thin-film transistors using amorphous oxide semiconductors. Nature 2004;432:488–92.

[3] Paine D, Whitson T, Janiac D, Beresford R, Yang C, Lewis B. A study of low temperature crystallization of amorphous thin film indium–tin–oxide. J Appl Phys 1999;85:8445–50.
[4] Moriga T, Fukushima A, Tominari Y, Hosokawa S, Nakabayashi I, Tominaga K. Crystallization process of transparent conductive oxides $Zn_kIn_2O_{k+3}$. J Synchrotron Radiat 2001;8:785–7.
[5] Utsuno F, Inoue H, Shimane Y, Shibuya T, Yano K, Inoue K, et al. A structural study of amorphous In_2O_{0033} films by grazing incidence x-ray scattering (GIXS) with synchrotron radiation. Thin Solid Films 2006;496:95–8.
[6] Cho D-Y, Song NJ, Hwang C, Jeong J, Jeong J, Mo Y-G. Local structure and conduction mechanism in amorphous In–Ga–Zn–O films. Appl Phys Lett 2009;94. 112112.
[7] Hoel C, Xie S, Benmore C, Malliakas C, Gaillard J-F, Poeppelmeier K. Evidence for tetrahedral zinc in amorphous $In_{2-2x}Zn_xSn_xO_3$ (a-ZITO). Z Anorg Allg Chem 2011;637:885–94.
[8] Proffit D, Ma Q, Buchholz D, Chang R, Bedzyk M, Mason T. Structural and physical property studies of amorphous Zn–In–Sn–O thin films. J Am Ceram Soc 2012;95:3657–64.
[9] Yang D, Lee J, Chung J, Lee E, Anass B, Sung N-E, et al. Local structure and local conduction paths in amorphous (In,Ga,Hf)-ZnO semiconductor thin films. Solid States Comm 2012;152:1867–9.
[10] Nomura K, Kamiya T, Ohta H, Uruga T, Hirano M, Hosono H. Local coordination structure and electronic structure of the large electron mobility amorphous oxide semiconductor In–Ga–Zn–O: experiment and ab initio calculations. Phys Rev B 2007;75:035212.
[11] Rosen J, Warschkow O. Electronic structure of amorphous indium oxide transparent conductors. Phys Rev B 2009;80:115215.
[12] Walsh A, Silva JD, Wei S-H. Interplay between order and disorder in the high performance of amorphous transparent conducting oxides. Chem Mater 2009;21:5119–24.
[13] Aliano A, Catellani A, Cicero G. Characterization of amorphous In_2O_3: an ab initio molecular dynamics study. Appl Phys Lett 2011;99:211913.
[14] Davis S, Gutierrez G. Structural, elastic, vibrational and electronic properties of amorphous Al_2O_3 from ab-initio calculations. J Phys Cond Matter 2011;23:495401.
[15] Kim M, Kang I, Park C. First-principle study of electronic structure of Sn-doped amorphous In_2O_3 and the role of O-deficiency. Curr Appl Phys 2012;12:S25–8.
[16] Ramzan M, Kaewmaraya T, Ahuja R. Molecular dynamics study of amorphous Ga-doped In_2O_3: a promising materials for phase change memory devices. Appl Phys Lett 2013;103:072113.
[17] Nishio K, Miyazaki T, Nakamura H. Universal medium-range order of amorphous metal oxides. Phys Rev Lett 2013;111:155502.
[18] Deng H-X, Wei S-H, Li S-S, Li J, Walsh A. Electronic origin of the conductivity imbalance between covalent and ionic amorphous semiconductors. Phys Rev B 2013;87:125203.
[19] Buchholz D, Ma Q, Alducin D, Ponce A, Yacaman M, Khanal R, et al. The structure and properties of amorphous indium oxide. Chem Mater 2014;26(18):5401–11.
[20] Kresse G, Hafner J. *Ab initio* molecular dynamics for liquid metals. Phys Rev B 1993;47:558–61.
[21] Kresse G, Hafner J. *Ab initio* molecular-dynamics simulation of the liquid-metal-amorphous-semiconductor transition in germanium. Phys Rev B 1994;49:14251–69.
[22] Kresse G, Furthmüller J. Efficiency of *Ab initio* total energy calculations for metals and semiconductors using a plane-wave basis set. Comput Mater Sci 1996;6:15–50.
[23] Kresse G, Furthmüller J. Efficient iterative schemes for *ab initio* total-energy calculations using a plane-wave basis set. Phys Rev B 1996;54:11169–86.
[24] Hohenberg P, Kohn W. Inhomogeneous electron gas. Phys Rev 1964;136:B864–71.
[25] Kohn W, Sham L. Self-consistent equations including exchange and correlation effects. Phys Rev 1965;140:A1133–8.
[26] Perdew J, Burke K, Ernzerhof M. Generalized gradient approximation made simple. Phys Rev Lett 1996;77:3865.
[27] Blöchl P. Projector augmented-wave method. Phys Rev B 1994;50:17953–79.
[28] Kresse G, Joubert D. From ultrasoft pseudopotentials to the projector augmented-wave method. Phys Rev B 1999;59:1758–75.
[29] Hoppe R. The coordination number – an "inorganic chameleon". Angew Chem Int Ed Engl 1970;9:25–34.
[30] Hoppe R, Voigt S, Glaum H, Kissel J, Muller H, Bernet K. A new route to charge distribution in ionic solids. J Less Common Met 1989;156:105–22.
[31] Hennek J, Smith J, Yan A, Kim M-G, Zhao W, Dravid V, et al. Oxygen "getter" effects on microstructure and carrier transport in low temperature combustion-processed a-InXZnO (X = Ga, Sc, Y, La) transistors. J Am Chem Soc 2013;135:10729–41.
[32] Khanal R, Buchholz D, Chang R, Medvedeva J. Structural properties of amorphous In–X–O with X = Zn, Ga, Sn, or Ge: ab-initio molecular dynamics study. unpublished manuscript.
[33] Medvedeva J, Hettiarachchi C. Tuning the properties of complex transparent conducting oxides: role of crystal symmetry, chemical composition, and carrier generation. Phys Rev B 2010;81:125116.
[34] Murat A, Medvedeva J. Electronic properties of layered multicomponent wide–band–gap oxides: a combinatorial approach. Phys Rev B 2012;85:155101.